https://doi.org/10.20965/ijat.2017.p0787

Paper:

Three-Dimensional Reconstruction by Time-Domain Optical Coherence Tomography Microscope with Improved Measurement Range

Shin Usuki*,†, Katsuaki Tamaki, and Kenjiro T. Miura****

*Research Institute of Electronics, Shizuoka University
3-5-1 Johoku, Naka-ku, Hamamatsu 432-8561, Japan
†Corresponding author, E-mail: usuki@shizuoka.ac.jp
**Graduate School of Engineering, Shizuoka University, Hamamatsu, Japan

[Received December 30, 2016; accepted April 14, 2017]

The objective of this research was to develop a three-dimensional (3D) reconstruction system based on a time-domain optical coherence tomography (OCT) microscope. One of the critical drawbacks of OCT microscopes is that their axial measurement ranges are typically limited by their depths of field (DOFs), which are determined by the numerical apertures of their objective lenses and the central wavelengths of their light sources. If a low-coherence interference fringe is far outside the DOF, the measurement accuracy inevitably decreases, regardless of how well-adjusted the reference mirror is. To address this issue and improve the axial measurement range of the OCT microscope in this study, an object-scanning measurement scheme involving a Linnik interferometer was developed. To calibrate the system in the proposed technique, image post-processing is performed for a well-conditioned state to ensure that a low-coherence interference fringe is generated within the DOF, enabling 3D objects with high-aspect-ratio structures to be scanned along the axial direction. During object-scanning, this state is always monitored and is corrected by adjusting the reference mirror. By using this method, the axial measurement range can be improved up to the working distance (WD) of the objective lens without compromising the measurement accuracy. The WD is typically longer than 10 mm, while the DOF of the microscope is around 0.01 mm in general, although it varies depending on the imaging system. In this report, the experimental setup of a 3D reconstruction system is presented, a series of experimental verifications is described, and the results are discussed. The axial measurement range was improved to at least 35 times that of a typical OCT microscope with identical imaging optics.

Keywords: three-dimensional reconstruction, three-dimensional measurement, optical coherence tomography, optical microscopy

1. Introduction

In recent years, the nano- and micro-manufacturing industries have progressed rapidly to meet the requirements of advanced technology and scientific research interests. In particular, three-dimensional (3D) printing and ultrahigh-precision machining technologies can enable significant improvements in several aspects of manufacturing, including accuracy, throughput, and degrees of freedom.

Furthermore, in the inspection process, geometric measurements and computational performance analyses are essential sources of feedback [1]. Thus, 3D reconstructions for geometric modeling and numerical simulations based on computer-aided engineering software are becoming increasingly important. By using 3D reconstruction methods to develop precise geometric models of in-line products, acceptable and defective products can be classified appropriately. Consequently, more efficient manufacturing systems can be constructed and more advanced technologies can be realized. Furthermore, in biomedical applications, 3D models are essential to quantitively measure and control the growth of cells.

To perform nano- and micro-scale 3D reconstructions, conventional 3D microscopic measurement techniques such as laser scanning confocal microscopy [2], scanning electron microscopy [3], and scanning probe microscopy [4] can be employed. The applicability of these techniques to industrial applications is limited because high-throughput, non-destructive, 3D measurements are necessary for product inspection, and these properties are difficult to achieve with conventional measurement systems. Optical microscopy is one potential means of realizing these characteristics simultaneously because it is non-destructive and can provide parallel imaging with an area image sensor for high-speed measurements. Especially in optical measurements, if a coherent light source is used, advanced interferometry can be performed [5]. Interferometry can be applied to measurement systems to enable the acquisition of not only the intensity of light, but also its phase, which includes 3D information about the investigated object [6].

In general, reconstructing 3D geometric information by performing optical microscopy is challenging because the imaging depth of field (DOF) is very shallow. Furthermore, parallax is nonexistent because the imaging system used in optical microscopy is based on orthographic projection. Therefore, an image-stacking technique, namely, the shape-from-focus method [7], is typically used to obtain the depth information of the object to be measured. The shape-from-focus method is time-consuming as numerous images must be acquired, making this technique unsuitable for industrial applications. Computational microscopy [8] is an effective means of overcoming this drawback, because it involves a computational problem rather than a physical one and specific computations to improve the measurement performance, such as the computation of the space-bandwidth product [9]. Optical light-field microscopy [10], a computational imaging technique with an expanded DOF and digital refocusing ability, can also be used to avoid the aforementioned drawbacks. The spatial resolution initially yielded by light-field microscopy is low, but it can be improved by using a sub-pixel super-resolution method [11]. However, even when this method is employed, the 3D reconstruction performance is insufficient for practical use because of its low sensitivity, which impedes the measurement of weak light [12].

Hence, in this study, we explored the possibility of using time-domain optical coherence tomography (OCT) [13] as an alternative 3D reconstruction method. Time-domain OCT is a well-known technique for cross-sectional tissue imaging and performing 3D measurements of reflective objects, therefore, its applications range from biomedical analysis to ultrahigh-precision manufacturing. In OCT, an incoherent light source and coherence gating are employed to enable the absolute measurement of the optical path length difference (OPD) between two arms in an interferometric optical system. Typically, OCT is used simultaneously with optical microscopy to achieve micron-scale-resolution measurements in every 3D direction. In this case, the lateral measurement range corresponds to the field of view (FOV) in optical microscopy, which is typically a few millimeters, although it varies depending on the imaging system. The axial measurement range, however, is limited by the DOF, which is determined by the numerical aperture (NA) of the objective lens and the central wavelength of the light source. In this situation, the effective axial measurement range is nearly 10 times as long as the DOF. If a low-coherence interference fringe is far outside the DOF, the measurement accuracy inevitably decreases, regardless of how well-adjusted the reference mirror is. Therefore, the axial measurement range is of sub-millimeter order, i.e., considerably shorter than the lateral measurement range, which implies that 3D objects with high-aspect-ratio structures cannot be measured in such situations. As one possible method of improving the axial measurement ranges of OCT microscopes, we propose employing an object-scanning measurement scheme involving a Linnik interferometer [14].

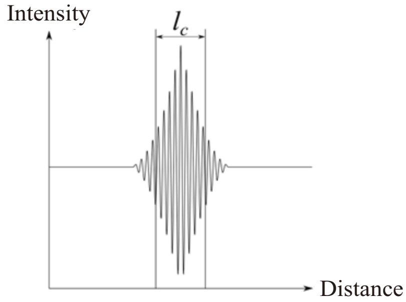

Fig. 1. Interference signal in OCT.

This paper introduces the proposed method in detail, describes the experimental setup used to investigate the 3D reconstruction system, and presents a discussion of the experimental results.

2. Methodology

2.1. OCT Microscope

In this study, we focused on using a time-domain OCT microscope to reconstruct the 3D shape of a micro-scale object. Conventional optical microscopy is not usable in situations where the signal-to-noise ratio (SNR) is low or the light reflected from the object is weak, e.g., if the object is small, has low reflectivity, or is located on an incline relative to the viewpoint. OCT microscopes do not experience these problems as they detect not only the intensity of light reflected from objects but also interference signals. Thus, OCT microscopes are more sensitive than conventional optical microscopes. The interference fringe contrast C is given by

$$C = \frac{2\sqrt{O}\cdot\sqrt{R}}{O+R}, \quad \text{(1)}$$

where O and R are the intensities of the light reflected by the object and the reference light, respectively. Even if O is reduced to 1% of its original value, 20% of the original C remains, which implies that an OCT microscope can provide a sensitivity and SNR that are sufficiently high to facilitate precise measurements.

In time-domain OCT, a low-coherence light source is employed for a specific interference signal (see **Fig. 1**), which enables absolute measurements of the OPD. The full-width at half-minimum of the envelope of a low-coherence interference fringe l_c is given by

$$l_c = \frac{2\ln}{\pi}\cdot\frac{\lambda_0^2}{\Delta\lambda}, \quad \text{(2)}$$

where λ_0 and $\Delta\lambda$ are the central wavelength and spectral width of the light source, respectively, and l_c is equivalent to the coherence length of the light source.

Three types of interferometers can be used for OCT [14]: Michelson, Mirau, and Linnik interferometers. Although each type has its advantages and disadvantages, Linnik interferometers are relatively easy to employ for low-cost, high-precision, 3D measurements. The com-

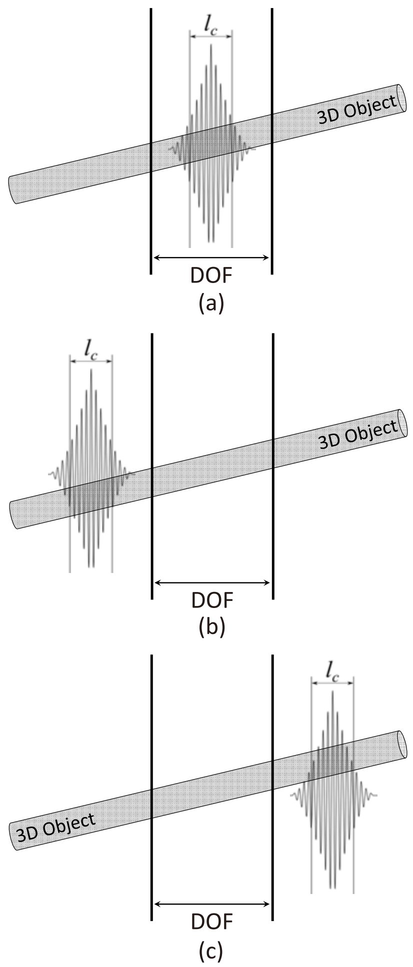

Fig. 2. Relationship between a 3D object with a high-aspect-ratio structure, microscope DOF, and low-coherence interference fringe in OCT. (a) interference occurring within or near the DOF. (b) and (c) reference mirror far outside the DOF.

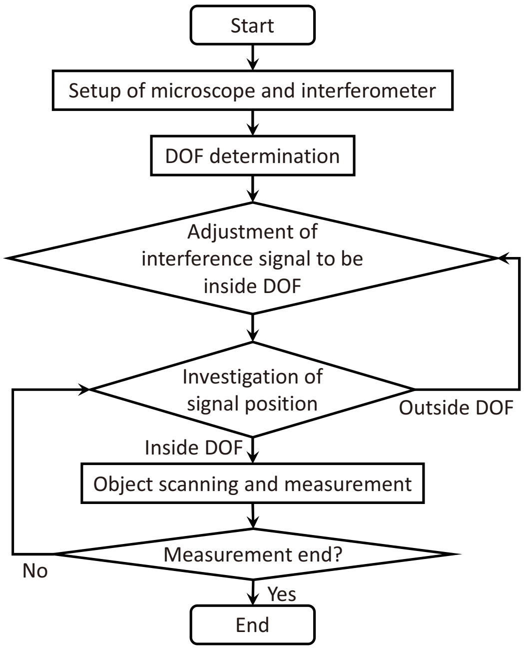

Fig. 3. Object-scanning procedure in the OCT measurement technique.

mon drawback of these three types of interferometers is that the resulting axial measurement range is short because it is limited by the DOF of the optical microscope, which is given by

$$DOF = \frac{\lambda_0}{2NA^2}, \quad . \ . \ . \ . \ . \ . \ . \ . \ . \ . \ . \ . \ . \ . \quad (3)$$

where λ_0 and NA are the central wavelength of the light source and the NA of the objective lens, respectively. The NA is given by the following equation.

$$NA = n \sin\theta, \quad . \ . \ . \ . \ . \ . \ . \ . \ . \ . \ . \ . \ . \ . \quad (4)$$

where n represents the refractive index of the medium between the objective lens and the object and θ is the aperture half-angle of the objective. **Fig. 2** shows a schematic of the relationship between a 3D measuring object with a high-aspect-ratio structure, DOF, and low-coherence interference fringe. In **Fig. 2**, they all exhibit a spatial dimension and are horizontally placed so they are comparable along the optical axis. The OCT measurements are usually performed by scanning the reference mirror along the axial direction. If the interference occurs within or near the DOF (see **Fig. 2(a)**), the OCT microscope performs sufficiently well. However, if the displacement of the reference mirror is far outside the DOF (see **Figs. 2(b)** and **(c)**), the fringe contrast, which indicates the measurement accuracy, is reduced because of the defocusing of the image outside the DOF. Consequently, the axial measurement range is limited by the DOF of the microscope.

2.2. Object-Scanning Scheme in OCT

To address the problem described above, we developed an object-scanning scheme based on an OCT microscope for the 3D reconstruction of objects with relatively high aspect ratios. The low-coherence interference fringe must be inside the DOF during object-scanning, otherwise, a sufficient fringe contrast cannot be achieved. The detailed procedure of the proposed method is depicted in **Fig. 3**. First, the OCT microscope with the Linnik interferometer is set-up by focusing on a microscope calibration target such as a USAF1951. Secondly, the experimental DOF and fine focus position are determined by scanning the target along the axial direction. Then, by adjusting the reference mirror, the interference fringe signal position is checked to determine whether the fringe is inside or outside the determined DOF. If it is inside, object-scanning starts and the measurements are performed; otherwise, the reference mirror must be readjusted. These processes are repeated during scanning so the fringe contrast will be sufficiently high for each measurement. This technique is rapid and smooth as every process is performed by the computational image processing of the acquired images.

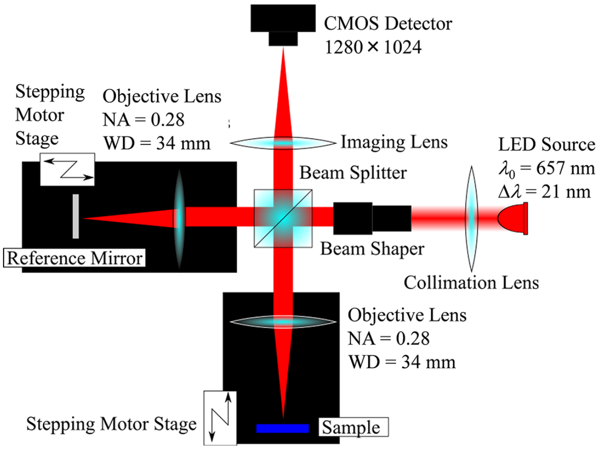

Fig. 4. Schematic diagram of the time-domain OCT microscope and Linnik interferometer.

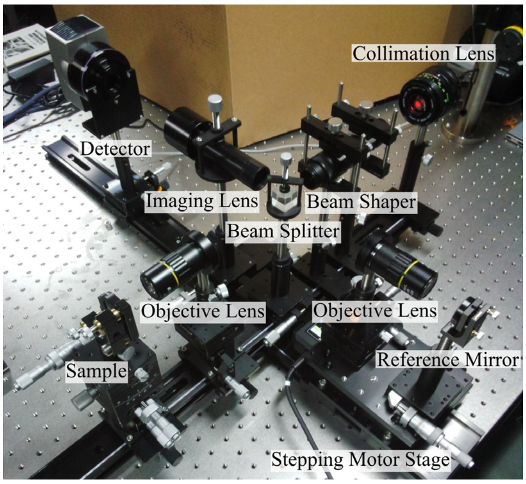

Fig. 5. Experimental setup of the object-scanning OCT microscope and Linnik interferometer.

3. Development

3.1. Object-Scanning Time-Domain OCT Microscope with Linnik Interferometer

To examine the abovementioned method experimentally, we developed an experimental setup involving a time-domain OCT microscope and Linnik interferometer. **Figs. 4** and **5** present a schematic diagram and photograph of the optical system, respectively. In this setup, a light-emitting diode (LED) with $\lambda_0 = 657$ nm and $\Delta\lambda = 21$ nm is employed as the light source for the OCT microscope. The LED light is well-collimated and homogenized by a collimation lens and beam shaper to maximize the interference contrast throughout the FOV of the microscope. Then, a beam splitter divides the light into two beams, which propagate along the two arms of the interferometric system. The beams are incident on the sample and reference sides of the objective lens and thereby illuminate the microscope. The light reflected by the sample and reference mirror is imaged on a complementary metal oxide semiconductor (CMOS) detector through the objective lens and imaging lens. At the same time as this imaging

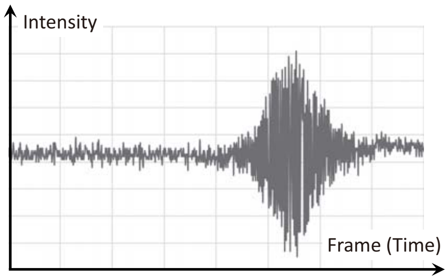

Fig. 6. Relationship between the low-coherence interference signal intensity detected at one pixel in the CMOS image and the acquired image frame.

process, a low-coherence interference fringe is generated on the detector if the OPD between the two arms is shorter than the coherence length of the light source, which was determined to be 9.1 μm based on Eq. (2). The NA and working distance (WD) of the objective lens were found to be 0.28 and 34 mm, respectively. Accordingly, the DOF and effective axial measurement range were calculated to be approximately 4.2 μm, by using Eq. (3), and 42 μm, respectively. Once the reference mirror is placed at the focus in this method, the distance between the mirror and the objective is fixed to ensure that the low-coherence interference fringe is inside the DOF. Then, the object-scanning and OCT measurement processes are started.

3.2. Interference Signal Processing Algorithm for OCT Measurement

In the developed time-domain OCT microscope, the interference signal is detected as an image sequence. The signal intensity at each image pixel varies depending on its image frame, which corresponds to its acquisition time. **Fig. 6** shows an example of the relationship between the low-coherence interference signal intensity detected at one pixel in a CMOS image and the acquired image frame. This relationship is referred to as the low-coherence interference signal. A flat mirror surface inclined by 10° with respect to the plane perpendicular to the optical axis was employed as the sample in the developed microscope. In the typical time-domain OCT measurement process, the image frame with the maximum intensity is assigned to be that at which the OPD between the two interferometer arms is zero. One means of performing this estimation is the intensity center of gravity method; however, the dispersion of the values estimated using this method is insufficient to enable high-precision measurements to be acquired. A depth map of the measured surface profile of the inclined mirror with the intensity center of gravity method is presented in **Fig. 7**, while **Fig. 8** depicts the line profile obtained along the red line in **Fig. 7** as well as the Pearson correlation coefficient R^2 of the linear approximation. As the mirror surface was almost flat, R^2 was expected to be close to unity. However, R^2 was estimated to be 0.9917 in this experiment, indicating the presence of a substantial error. To improve the estimation accuracy, a Savitzky–Golay filter [15] was

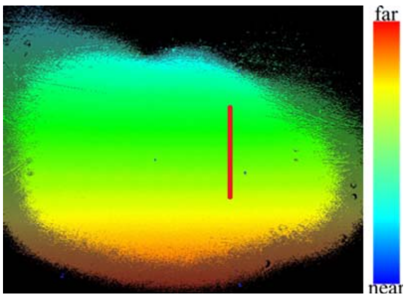

Fig. 7. Depth map of the measured surface profile of the inclined mirror estimated using the intensity center of gravity method.

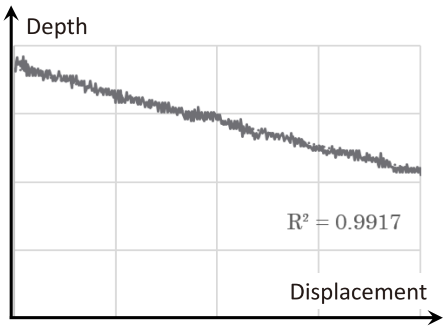

Fig. 8. Line profile along the red line in **Fig. 7** and the R^2 value of the linear approximation.

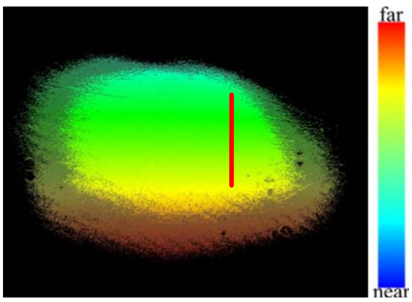

Fig. 9. Surface profile of the inclined mirror, which was estimated using the Savitzky–Golay filter and the moving least squares method.

employed as a low-pass filter to enable the data characteristics to be more stably maintained, and the moving least squares method [16] was applied for the peak position estimation to increase the robustness against noise. **Figs. 9** and **10** respectively illustrate the depth map of the measured surface profile of the inclined mirror and the line profile along the red line in **Fig. 9**, which was obtained using the proposed estimation method. The estimation accuracy is improved, as evidenced by the smoother line profile and R^2 value of 0.9977, which is closer to unity than that obtained using the conventional intensity center of gravity method. In addition, the estimation results visualized using the 3D point cloud viewer are presented in **Fig. 11**. The shape of the inclined mirror surface seems to have been reconstructed appropriately.

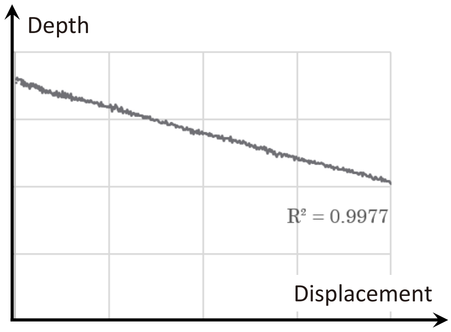

Fig. 10. Line profile along the red line in **Fig. 9** and the R^2 value of the linear approximation.

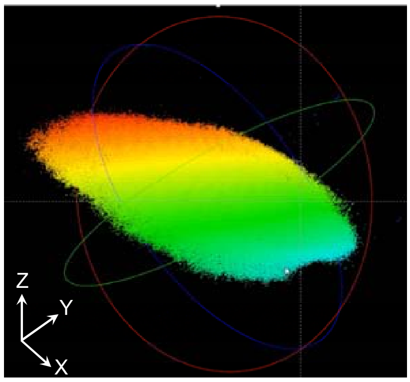

Fig. 11. Reconstructed 3D shape of the inclined mirror surface.

4. Results and Discussion

4.1. Measurement of a Micro-Sized Machining Tool with High-Aspect-Ratio Structures Using the Developed OCT Microscope

This section describes the experimental verification of the developed time-domain, object-scanning OCT microscope mentioned in Section 3.1, which was conducted using a micro-sized machining tool blade with a high-aspect-ratio structure as the sample. The experimental conditions and the 3D object that was measured are presented in **Table 1** and **Fig. 12**, respectively. The blade of the micro-sized machining tool had both convex and concave structures, which differed in height by 150 μm. This difference is far greater than the effective axial measurement range of a conventional OCT microscope. Therefore, the scanning range was set to 180 μm, corresponding to 1800 frames with a scanning speed of 0.1 μm/frame. In this situation, however, the FOV of the microscope was too narrow to cover both structures of the tool blade. Consequently, the lateral position of the object was changed at frame 900 so its entire structure could be measured during one scan. **Fig. 13** presents an example of an image sequence acquired by axially scanning the object. The fringe contrast of the low-coherence interference is maximized around frames 300 and 1500, which correspond to the concave and convex structures, respectively, of the tool blade. Ideally, the difference between the concave and convex frames would be around 1500, but

Table 1. Experimental conditions of the time-domain object-scanning OCT microscope.

Parameter	Value
Central wavelength of the light source	657 nm
Spectral width of the light source	21 nm
Coherence length of the light source	9.1 μm
Magnification of the objective lens	10x
NA of the objective lens	0.28
WD of the objective lens	34 mm
DOF of the imaging system	4.2 μm
Effective axial measurement range of OCT	42 μm
Resolution of the CMOS image sensor	1280$\times$1024
Pixel size of the CMOS image sensor	3.6 μm
Object scanning stage step size per frame	0.1 μm/frame
Total object scanning range	180 μm

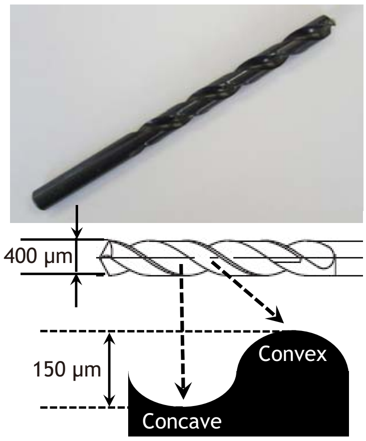

Fig. 12. Micro-sized machining tool blade with a high-aspect-ratio structure, which was used as the 3D object.

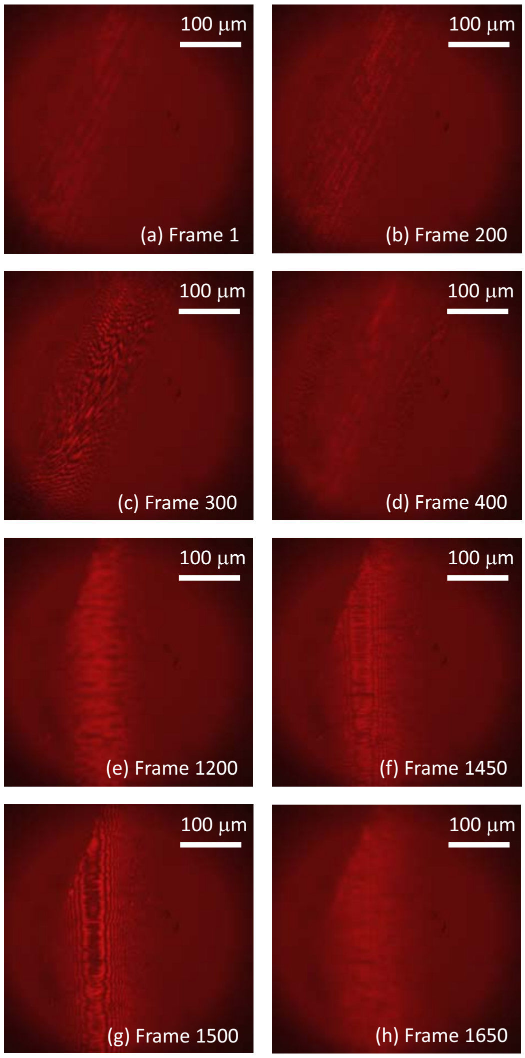

Fig. 13. Image sequence acquired by axially scanning the object.

considerable errors were caused by the insufficient positioning accuracy of the stepping motor stage and changes in the lateral position of the object.

4.2. 3D Reconstruction of the Micro-Sized Machining Tool Blade

The signal processing algorithm described in Section 3.2 was applied to the acquired image sequence to perform 3D reconstruction of the object. **Figs. 14** and **15** depict the depth map and 3D view of the results reconstructed for the concave and convex structures, respectively. As previously mentioned, the absolute height difference between the concave and convex structures could not be measured, but the blade structure can still be seen in the reconstruction results. The axial measurement range was improved to at least 35 times that of a typical OCT microscope with the same imaging optics. Thus, the proposed OCT microscope system can be used to measure 3D objects with high-aspect-ratio structures. The reconstruction results, however, were influenced by noise, which can be seen in both **Figs. 14** and **15**. The noise is considered to be caused by the deformation of the direct-current (DC) component in the fringe signal of the proposed OCT system. The DC components of the conventional and proposed OCT microscopes are indicated by red lines in **Fig. 16**. In conventional OCT, the measured object is fixed and the reference mirror is scanned, and the contrast is uniform in each focusing image, so the DC component is stably flat. Conversely, the focusing image contrast varies during the axial scanning of the object in the proposed OCT microscope, and the defocus blur influences the neighboring pixels in each image, so the DC component may be deformed. One means of solving this problem is the direct smoothing of the 3D point cloud, while another, more intrinsic solution involves correcting the deformation so it becomes flat by using signal processing techniques.

5. Conclusion

In this report, we presented a 3D reconstruction system based on a time-domain OCT microscope with an improved axial measurement range. The proposed reconstruction technique involves object-scanning to improve the axial measurement range up to the WD of the objective lens, which is considerably longer than that of a con-

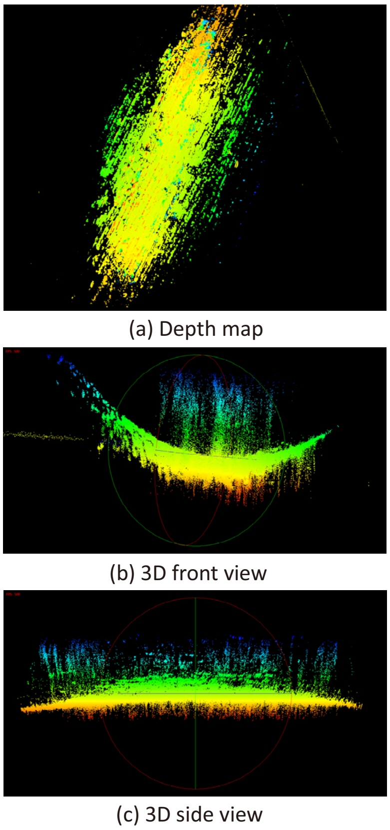

Fig. 14. 3D reconstruction of the concave structure of the micro-sized machining tool blade.

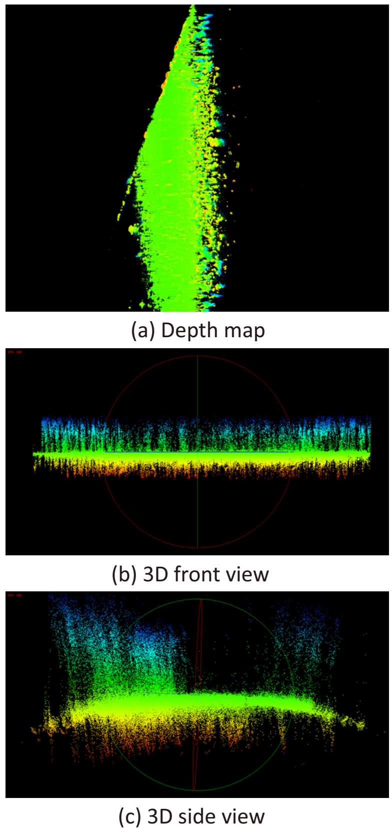

Fig. 15. 3D reconstruction of the convex structure of the micro-sized machining tool blade.

ventional OCT microscope. An experimental setup and fringe signal processing algorithm were developed; then, a series of experiments was performed, in which the concave and convex structures of a machining tool blade were reconstructed in 3D. This object has a relatively high aspect ratio and is difficult to measure with a conventional OCT microscope as the effective axial measurement range is only about 10 times as long as the DOF of the imaging system. The developed OCT system yielded a range that was substantially greater than that achieved by the conventional system, and the tool blade was measured during a single scan. Even though the originally developed fringe signal processing algorithm with improved estimation accuracy was applied, the reconstruction results remained noisy because of the DC component deformation of the fringe signal. In future work, theoretical analysis of the wider measurement range could be performed, and deformation correction could be applied to further improve the 3D reconstruction system.

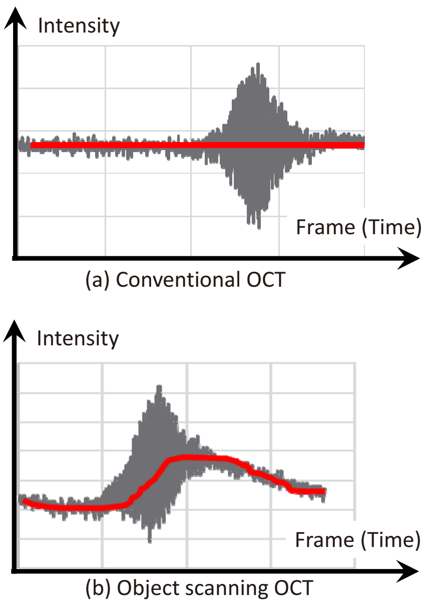

Fig. 16. Red lines representing the (a) flat DC component of the fringe signal in conventional OCT and (b) deformed DC component in the proposed OCT method.

Acknowledgements

This work was supported by JSPS KAKENHI Grant-in-Aid for Young Scientists (A), Grant Number 16H06063.

References:

[1] S. Usuki and K. T. Miura, "Nano-micro geometric modeling using microscopic image," Key Engineering Materials, Vol.523-524, pp. 345-349, 2012.

[2] N. S. Claxton, T. J. Fellers, and M. W. Davidson, "Laser scanning confocal microscopy," Department of Optical Microscopy and Digital Imaging National High Magnetic Field Laboratory, Florida State University, Unpublished (http://www.olympusfluoview.com/theory/LSCMIntro.pdf), 2005.

[3] J. Pawley, "The development of field-emission scanning electron

microscopy for imaging biological surfaces," Scanning, Vol.19, No.5, pp. 324-336, 1997.

[4] R. Howland and L. Benatar, "A Practical Guide to Scanning Probe Microscopy," Park Scientific Instruments, 1993.

[5] T. Yidong, W. Weiping, X. C. Xin, and Z. Shulian, "Laser confocal feedback tomography and nano-step height measurement," Nature Scientific Reports 3, Article number: 2971, 2013.

[6] H. Schreiber and J. H. Bruning. "Phase shifting interferometry," Optical Shop Testing, Third Edition, pp. 547-666, 2006.

[7] S. K. Nayar and Y. Nakagawa, "Shape from focus," IEEE Trans. on Pattern Analysis and Machine Intelligence, Vol.16, No.8, pp. 824-831, 1994.

[8] L. Bian, J. Suo, J. Chung, X. Ou, C. Yang, F. Chen, and Q. Dai, "Fourier ptychographic reconstruction using Poisson maximum likelihood and truncated Wirtinger gradient," Nature Scientific Reports 6, Article number: 27384, 2016.

[9] A. W. Lohmann et al., "Space–bandwidth product of optical signals and systems," J. of the Optical Society of America A, Vol.13, No.3, pp. 470-473, 1996.

[10] M. Levoy, R. Ng, A. Adams, M. Footer, and M. Horowitz, "Light field microscopy," ACM Trans. on Graphics, Vol.25, No.3, pp. 924-934, 2006.

[11] S. Usuki and K. T. Miura, "High-resolution tolerance against noise imaging technique based on active shift of optical axis," Int. J. of Automation Technology, Vol.5, No.2, pp. 206-211, 2011.

[12] S. Usuki, M. Uno, and K. T. Miura, "Digital shape reconstruction of a micro-sized machining tool using light-field microscopy," Int. J. of Automation Technology, Vol.10, No.2, pp. 172-178, 2016.

[13] M. R. Hee et al., "Optical coherence tomography of the human retina," Archives of Ophthalmology, Vol.113, No.3, pp. 325-332, 1995.

[14] A. Dubois et al., "High-resolution full-field optical coherence tomography with a Linnik microscope," Applied Optics, Vol.41, No.4, pp. 805-812, 2002.

[15] M. J. Savitzky and E. Golay, "Smoothing and differentiation of data by simplified least-squares procedures," Analytical Chemistry, Vol.36, pp. 1627-1639, 1964.

[16] S. Fleishman, D. Cohen-Or, and C. T. Silva, "Robust moving least-squares fitting with sharp features," ACM Trans. on Graphics, Vol.24, No.3, pp. 544-552, 2005.

Name:
Shin Usuki

Affiliation:
Research Institute of Electronics, Shizuoka University

Address:
3-5-1 Johoku, Naka-ku, 432-8561 Hamamatsu, Japan

Brief Biographical History:

2002 Received B.Eng. from the Department of Precision Engineering, the University of Tokyo

2004 Received M.Eng. from the Department of Precision Engineering, the University of Tokyo

2008 Received D.Eng. from the Department of Precision Engineering, the University of Tokyo

2008-2013 Assistant Professor in the Division of Global Research Leaders, Shizuoka University

2013- Associate Professor in the Research Institute of Electronics, the Department of Mechanical Engineering, the Faculty of Engineering, Shizuoka University

Main Works:

- S. Usuki, M. Uno, and K. T. Miura, "Digital Shape Reconstruction of a Micro-Sized Machining Tool Using Light-Field Microscopy," Int. J. of Automation Technology, Vol.10, No.2 pp. 172-178, 2016.

Membership in Academic Societies:

- Japan Society for Precision Engineering (JSPE)
- Japan Society of Mechanical Engineers (JSME)

Name:
Katsuaki Tamaki

Affiliation:
Department of Mechanical Engineering, Shizuoka University

Address:
3-5-1 Johoku, Naka-ku, 432-8561 Hamamatsu, Japan

Brief Biographical History:

2016 Received B.Eng. from the Department of Mechanical Engineering, Shizuoka University

Name:
Kenjiro T. Miura

Affiliation:
Department of Information and Technology, Graduate School of Science and Technology, Shizuoka University

Address:
3-5-1 Johoku, Naka-ku, 432-8561 Hamamatsu, Japan

Brief Biographical History:

1982 Obtained B.Eng. from the University of Tokyo

1984 Obtained M.Eng. from the University of Tokyo

1991 Obtained Ph.D. from Cornell University

2003- Full Professor in Department of Mechanical Engineering, Faculty of Engineering and Department of Information Science and Technology, Graduate School of Science and Technology (joint appointment) of Shizuoka University

Main Works:

- K. T. Miura and R. U. Gobithaasan, "Aesthetic Curves and Surfaces in Computer Aided Geometric Design," Int. J. of Automation Technology, Vol.8, No.3, pp. 304-316, 2014.

Membership in Academic Societies:

- Japan Society for Precision Engineering (JSPE)
- Japan Society of Mechanical Engineers (JSME)
- Information Processing Society of Japan (IPSJ)